A New Focus on Groundwater–Seawater Interactions
(Proceedings of Symposium HS1001 at IUGG2007, Perugia, July 2007). IAHS Publ. 312, 2007.

Simulation of submarine groundwater discharge salinity and temperature variations: implications for remote detection

ALYSSA M. DAUSMAN[1,2], CHRISTIAN D. LANGEVIN[1] & MICHAEL C. SUKOP[2]

1 *US Geological Survey-Florida Integrated Science Center, 3110 SW 9th Avenue, Fort Lauderdale, Florida 33315, USA*
adausman@usgs.gov

2 *Florida International University-Department of Earth Sciences, Miami, Florida 33199, USA*

Abstract A hydrological analysis using a numerical simulation was done to identify the transient response of the salinity and temperature of submarine groundwater discharge (SGD) and utilize the results to guide data collection. Results indicate that the amount of SGD fluctuates depending on the ocean stage and geology, with the greatest amount of SGD delivered at low tide when the aquifer is in direct hydraulic contact with the ocean. The salinity of SGD remains lower than the ocean throughout the year; however, the salinity difference between the aquifer and ocean is inversely proportional to the ocean stage. The temperature difference between the ocean and SGD fluctuates seasonally, with the greatest temperature differences occurring in summer and winter. The outcome of this research reveals that numerical modelling could potentially be used to guide data collection including aerial surveys using electromagnetic (EM) resistivity and thermal imagery.

Key words submarine groundwater discharge

INTRODUCTION

In coastal areas, submarine groundwater discharge (SGD) is a topic of increasing concern to marine scientists, primarily because terrestrially derived groundwater can release nutrients and other potentially harmful contaminants into ecologically sensitive marine environments (Finkl & Krupa, 2003; Taniguchi *et al*., 2002). It is difficult to quantify SGD, however, because spatial variations in recharge, aquifer hydraulic properties, tides, and other complicating factors can substantially affect patterns and rates of groundwater flow to the ocean. The presence of geological heterogeneity, for example, can complicate the measurement of SGD (Bokuniewicz *et al*., 2003).

Improved aerial survey techniques that utilize electromagnetic (EM) and thermal imagery provide a direct means to map zones of increased SGD (Weiss *et al*., 2005). EM methods can be used to detect subsurface salinity differences, whereas thermal imagery can detect small water temperature variations at the sea surface (greater than 0.08°C in calm seas). Therefore, it is possible to detect SGD with an aerial survey if the salinity or temperature difference between SGD and the ocean is relatively large. The best time to conduct an aerial survey is when salinity and temperature differences between SGD and surface water are the greatest.

Variable-density numerical models are often used for management purposes to simulate groundwater flow in coastal aquifers, including saltwater intrusion and SGD. A deep (~3 km) model of North Carolina was developed to investigate fresh and saline SGD, as well as geothermal convection in a coastal setting (Wilson, 2005). Langevin (2003) used a variable-density flow and transport model to quantify rates of fresh SGD into Biscayne Bay in southern Florida. Smith & Zawadski (2003) calibrated a two-dimensional cross-sectional model to seepage measurements in the northeastern Gulf of Mexico. Previous research with data collection and modelling has also shown that seasonality can affect the amount of SGD resulting from water-table changes (Michael *et al*., 2005). However, few numerical modelling studies, if any, have been designed specifically to guide data collection efforts.

The purpose of this paper is to demonstrate how a numerical model can be used to guide data collection efforts in studies of SGD. A variable-density numerical model was developed using generalized hydrological conditions for southeastern Florida to determine when and where SGD rates are the greatest and to quantify expected temperature and salinity differences between groundwater and ocean water. The model is unique in that it represents SGD characteristics, including salinity and temperature, at short-term (tidal) and longer-term (seasonal) time scales. Results from the model are used to provide insight into optimal times to perform aerial surveys.

METHODS

To evaluate transient variations in the salinity and temperature of SGD, a 2-D cross-sectional model was developed using idealized hydrogeological conditions and hydraulic parameters common to southeastern Florida (Dausman & Langevin, 2005) (Figs 1 and 2). The numerical model is intended to represent generalized flow conditions in the Biscayne aquifer in southeastern Florida rather than one specific location. The data used to develop the model were obtained from various places in southeastern Florida including Miami-Dade, Palm Beach, and Broward Counties (Fig. 1). The 2-D vertical cross-sectional model was aligned along a west-to-east groundwater-flow line perpendicular to the coastline. The model represents a 1-year period, from 1 January 1998 to 31 December 1998, using hourly stress periods. Consecutive simulations were run using head, salinity, and temperature from the previous model run until salinities and temperatures achieved dynamic equilibrium.

The SEAWAT code (Langevin *et al.*, 2003), which is a combined version of MODFLOW (McDonald & Harbaugh, 1988) and MT3DMS (Zheng, 1990), simulates variable-density flow driven by changes in salinity. A modified version of this code was used in this study to simulate density-dependent flow caused by changes in salinity, as well as simulate changes in temperature (Thorne *et al*., 2006).

The 2-D model grid contains 152 columns and 14 layers; each cell is 150 by 7.5 m. The active cells represent the Biscayne aquifer (Table 1), which is underlain by a low-permeability unit (represented with no-flow cells). The specified head cells along the sea floor represent the ocean. The ocean water levels and temperature values vary hourly according to measured data collected during 1998. The salinity value is specified at 35 parts per thousand (ppt). General-head boundary (GHB) cells on the

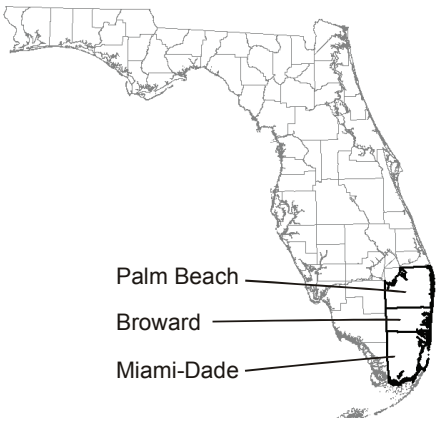

Fig. 1 Map of Florida with the three counties containing the Biscayne aquifer.

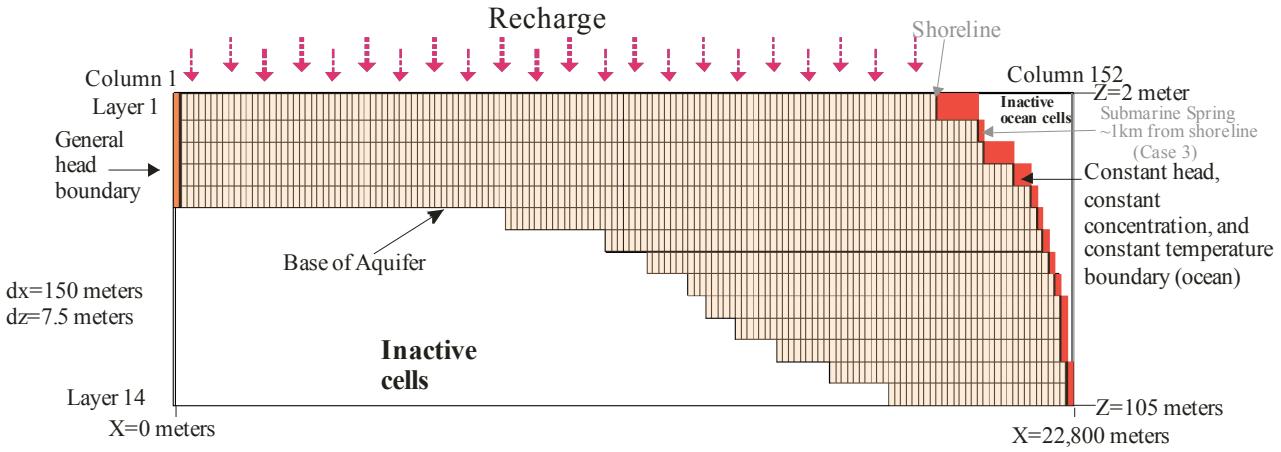

Fig. 2 Boundary conditions and finite difference model grid.

Table 1 Aquifer parameters used in the variable-density cross-sectional models (from Dausman & Langevin, 2005).

Parameter (units)	Parameter definition	Value
K_H (m/d)	Horizontal hydraulic conductivity	1150
K_v (m/d)	Vertical hydraulic conductivity	150
α_L (m)	Longitudinal dispersivity	3.0
α_T (m)	Transverse dispersivity	0.3
S_y (dimensionless)	Specific yield	0.1
S (dimensionless)	Storage	10^{-5}
n (dimensionless)	Porosity	0.1
D* (m^2/d)	Bulk thermal diffusivity	0.67996
μ (kg/(m d))	Equivalent freshwater viscosity	86.4
ρ_f (kg/m^3)	Density of fresh water	1000
ρ_s (kg/m^3)	Density of sea water	1025
$\frac{d\rho}{dC}$ (dimensionless)	Density change with concentration	0.7
$\frac{d\mu}{dC}$ (m^2/d)	Viscosity change with concentration	10^{-6}

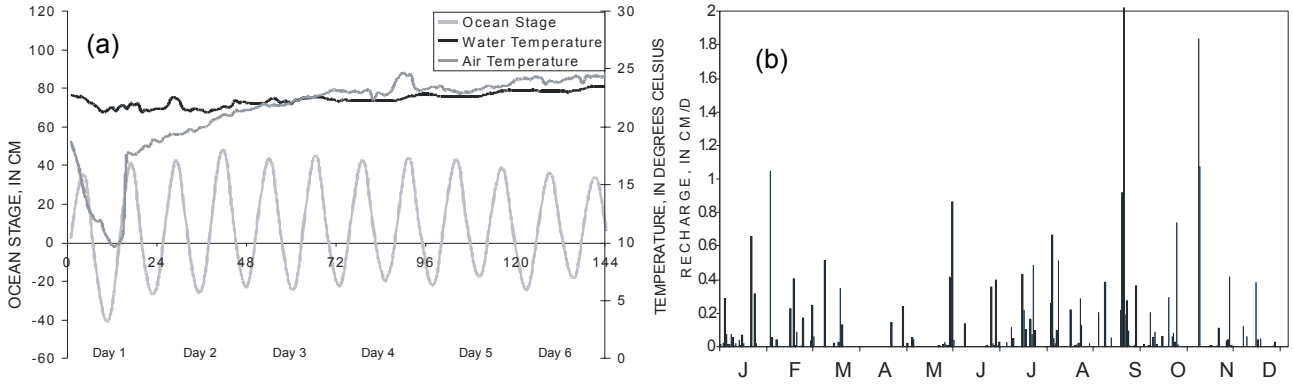

Fig. 3 (a) The first 6 days of the stage in the ocean boundary, temperature of the ocean boundary, and air temperature used in the recharge and general head boundary cells. (b) Model recharge.

western model boundary were used to represent hydraulic connection with the Florida Everglades. Assigned GHB heads, salinities, and temperatures were based on observed conditions. Net recharge, approximated as 15% of rainfall, changes daily; the temperature of recharge changes hourly according to measured air temperatures (Fig. 3(a), (b)).

Three scenarios were simulated to quantify different types of hydraulic connection with the ocean. In the first case, the Biscayne aquifer is in direct hydraulic connection with the ocean (Fig. 4). In Case 2, a low hydraulic conductivity layer is assigned along the sea floor (representing low-permeability marine sediments) to reduce the hydraulic connection with the ocean (Fig. 4). This low-permeability layer is included in the model by setting the vertical and horizontal hydraulic conductivities of the constant head cells (CHD) to a value of 0.05 m/d. In this approach, the thickness of the marine sediments is about one half of a cell thickness of each CHD cell. The storage of the low permeability layer is assumed to be the same as that of the aquifer, 10^{-5}. We did not test the effects of different storage values. However, the decrease in hydraulic conductivity of the low permeability layer results in a lower hydraulic diffusivity causing a damping of the ocean tides. Case 3 is identical to Case 2, except for the presence of a spring 1 km from the shoreline (column 137) (Figs 2 and 4). At this location, the Biscayne aquifer is in direct hydraulic connection with the ocean.

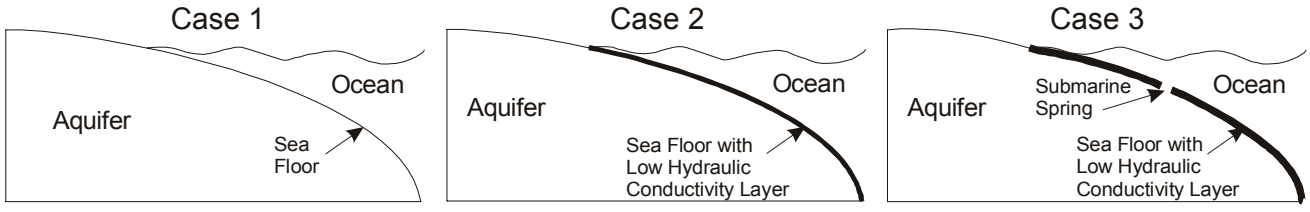

Fig. 4 Conceptual models of hydraulic connection between the aquifer and the ocean.

RESULTS

Simulation results include groundwater discharge rates (and salinities and temperatures) for each hourly stress period and for each model cell. These discharge rates were combined or averaged in different ways to highlight the differences between the three

cases. Rates to individual model cells are expressed in units of m/d. When discharge rates are combined, they are expressed in units of m^3/d per meter of shoreline (expressed as m^2/d), or in the case of a cumulative discharge, as m^3 per meter of shoreline.

Figure 5(a) shows the total SGD (calculated by summing the discharge for the ocean cells) as a function of time for the first 7 days of the simulation. The highest discharge rates (positive indicating flow from the aquifer into the ocean) occur during low tide; the lowest rates occur during high tide. As expected, the minimum and maximum discharges are a function of the hydraulic connection between the aquifer and the ocean. Case 1 has the highest discharge rates, ranging between about 150 and –150 m^2/d. Case 2 has the lowest discharge rates, ranging between 50 and –50 m^2/d. Because Case 3 contains hydraulic features of both cases 1 and 2, the discharge rates range between cases 1 and 2. The combined discharge totals for the entire simulation are shown in Fig. 5(b). The largest discharge occurs in Case 1, followed by cases 2 and 3, respectively. A mass balance analysis revealed that approximately the same amount of freshwater is discharged to the ocean for all three models; however, more seawater is recirculated in Case 1, resulting in a larger total.

Fresh recharge is applied to the top of the model. About 25% of that fresh recharge flows to the west and discharges to the western boundary. The remaining 75% discharges into the ocean. The type of hydraulic connection has a large effect on where SGD occurs in relation to the shoreline. The average annual rate of SGD was calculated for each ocean constant-head cell (Fig. 6). In Case 1, most of the SGD is into the first ocean cell. Case 1 also shows large components of recirculated seawater, observed as negative SGD rates farther offshore. The low hydraulic conductivity layer in Case 2 impedes SGD, forcing terrestrially-derived groundwater to discharge as far as 1.8 km from the shoreline. For Case 3, most of the SGD is concentrated into the cell representing the submarine spring; however, relatively low discharge rates are observed near the shoreline.

As shown in Fig. 6, SGD rates fluctuate between positive and negative values during a tidal cycle making it difficult to determine a net discharge rate. For this reason, the cumulative discharge (in m^3 per meter of shoreline) as a function of time was calculated for the first model cell representing the ocean (Fig. 7(a)). The final value of about 6,000 m^3/m of shoreline over the course of 1 year is equivalent to an average SGD rate of about 0.11 m/d (calculated from the 150-m cell width). Also

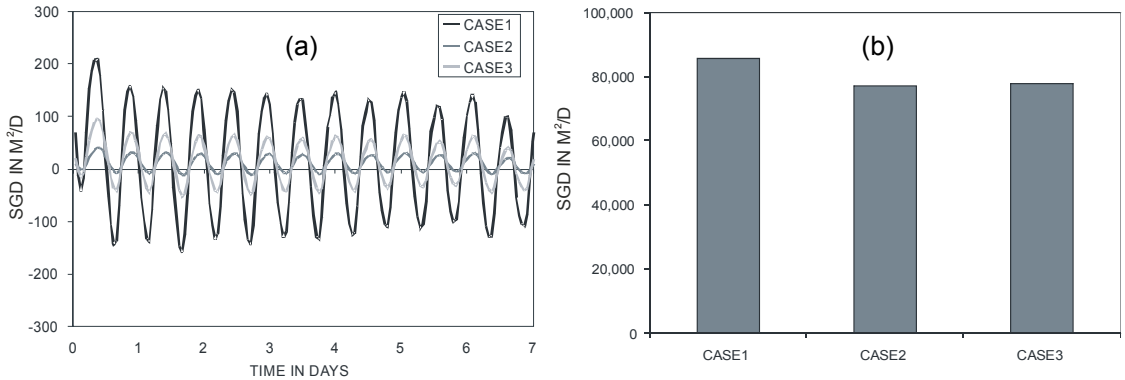

Fig. 5 (a) The sum of SGD for each case over time. The first 7 days of the model are shown. (b) The total amount of SGD for each case.

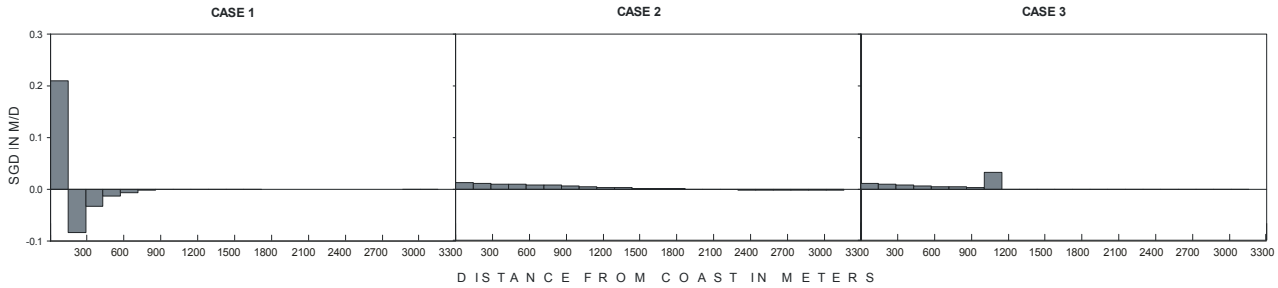

Fig. 6 Model results showing the annual average discharge with distance from the coast.

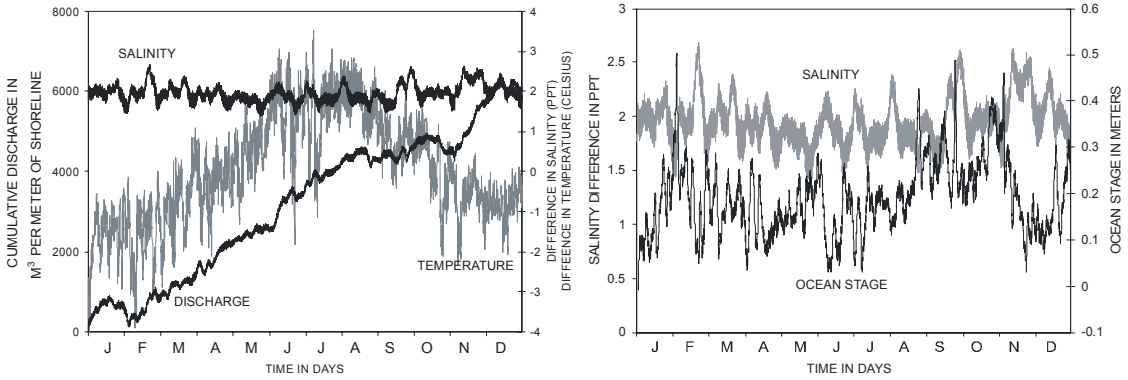

Fig. 7 (a) Cumulative discharge, the difference in salinity and the difference in temperature with time at the first cell representing the ocean for Case 1. (b) The difference in salinity and the ocean stage with time at the coast for Case 1.

shown in Fig. 7(a) are the temperature and salinity differences between the ocean and underlying aquifer cell at the shoreline. The average salinity difference is only about 2 ppt, indicating that most of the SGD for this case has near-seawater salinities. Fluctuations in salinity difference are primarily caused by fluctuations in ocean stage as shown by an inverse correlation (Fig. 7(b)); a higher ocean stage corresponds with a smaller difference in salinity between the aquifer and ocean.

The difference in temperature between the ocean and SGD fluctuates seasonally, with warmer groundwater discharging into the colder saline ocean in the winter (Figs 7(a) and 8(a)). During late summer, cooler groundwater discharges into the warmer ocean waters (Fig. 8(b)). Temperature differences between groundwater and the ocean are minimal during the spring and fall (Fig. 8(c)). In southern Florida, the ocean and rainfall are both warmer (~28ºC, assuming that rainfall temperature equals air temperature) during summer than during winter (~22ºC). Groundwater that is discharged to the coast remains at about 25ºC, which is a mixture of the older warmer and cooler waters from previous seasons. Because the ocean water temperature varies from about 22ºC in winter to 28ºC in summer, these are periods of greatest temperature difference between ocean waters and older mixed aquifer waters that are discharged to the coast.

Model results at low tide (when SGD rates and salinity differences are large) and in winter (when temperature differences between the ocean and aquifer are the largest) are shown in Fig. 9 for the three cases. Temperature and salinity differences are shown here with the SGD rates to give an indication of whether the discharge would be

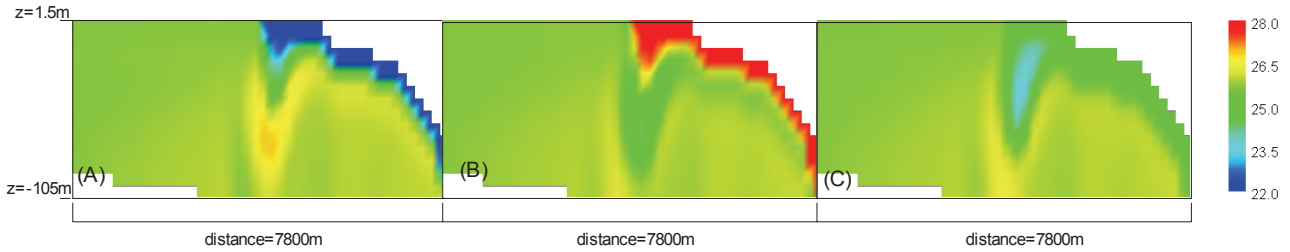

Fig. 8 Temperature (°C) for Case 1 during (A) winter, (B) summer and (C) spring.

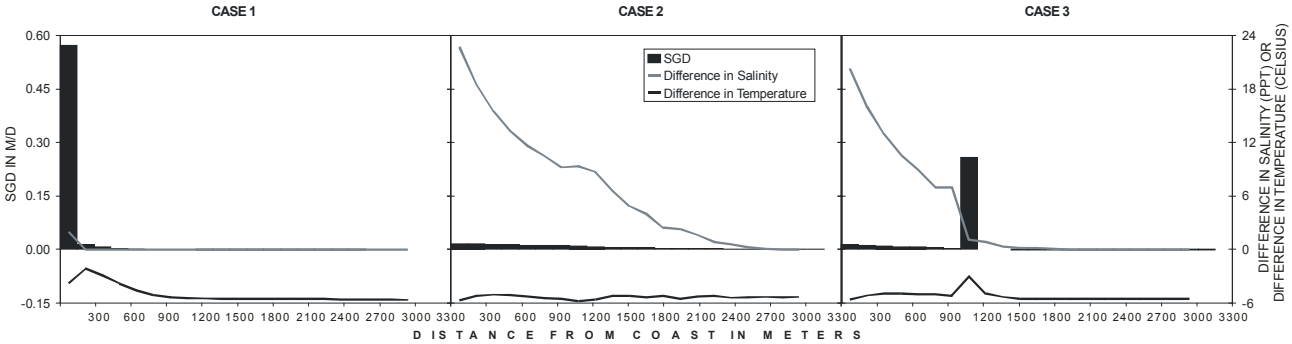

Fig. 9 Discharge, difference in salinity and difference in temperature *vs* distance from the coast, at low tide in winter.

detectable from an aerial survey (i.e. do the largest temperature and salinity differences correspond with the locations of largest discharge?). For Case 1, where most of the discharge is at the shoreline, the salinity difference is about 2 ppt and the temperature difference is about 3ºC. In Case 2, the fresh SGD is not concentrated near the shoreline, but discharged over a 1-km outflow face with distance from the coast. The low hydraulic conductivity layer in Case 2 impedes the flow of SGD and reduces the mixing of the aquifer and ocean waters. The reduced mixing results in a salinity difference between the ocean and aquifer of from 6 to 23 ppt across the outflow face, with the greatest difference near the shoreline (Fig. 9). However, differences in temperature between groundwater and the ocean in Case 2 stay relatively consistent at ~6ºC across the outflow face. Case 3 shows a relatively large amount of SGD at the submarine spring, where fresher groundwater is allowed to discharge to the spring. The increased mixing at the spring results in a decrease in the salinity difference between the ocean and aquifer to approximately 3 ppt at the main point of discharge. The temperature difference between the aquifer and ocean at the spring is approximately 3ºC (Fig. 9).

DISCUSSION

Variable-density groundwater flow models can be used to understand the complex nature of a coastal groundwater system. This analysis illustrates how the salinity, temperature and rate of SGD are affected by the hydraulic character of the coastal system from the geological setting to ocean characteristics. The results from this type of analysis can be used to help guide data collection efforts for studies of SGD.

Aerial surveys using EM resistivity are used to detect fresh SGD to the ocean. An EM resistivity survey has the ability to detect salinity variations at depth. During all times of the year, fresher groundwater is discharged to the ocean. However, the salinity difference between the aquifer and ocean is affected by the hourly and monthly ocean stage variations. The modelling for this research reveals that aerial EM surveys are best conducted at low tide and when ocean stages are at a relative low. This is when the difference in salinities between the aquifer and ocean are greatest (Figs 7(b) and 9). Therefore, the results from an aerial survey could potentially be improved by including expected ocean stage variations for the specific target area as part of the data collection plan.

An aerial survey using EM resistivity may or may not be successful depending upon the geology of the aquifer. An aquifer in direct hydraulic connection to the ocean, such as Case 1, may not have large enough salinity differences between the aquifer and ocean for an aerial survey to detect (a difference of only 2 ppt at the shoreline, decreasing to 0 ppt with distance from the shore). Case 2 contains a low hydraulic conductivity layer of sediments across the ocean floor. Although the sediments impede SGD and increase the zone of discharge over a larger area of the ocean floor, the difference in salinity between the ocean and aquifer waters is relatively high in this environment (up to 23 ppt), enabling likely detection by EM resistivity (Fig. 9). If there is a fracture in the low conductivity layer, resulting in a submarine spring, as in Case 3, the SGD across the ocean floor and at the spring may be high enough for detection by the survey as long as the salinity differences between the aquifer and ocean are relatively high, as in Fig. 9.

Data collection methods utilizing thermal imagery to quantify SGD are successful in calm waters where the temperature difference between the SGD and ocean waters is greater than 0.08ºC at the ocean surface. Thermal imagery cannot detect temperature variations below the surface; therefore, a larger temperature difference between the SGD and the ocean and a relatively large amount of SGD is necessary for detection. Thermal images should be collected at low tide when SGD is relatively high and at a location where SGD rates would be large enough to affect the ocean surface temperature. In southern Florida, thermal imagery surveys are best conducted during the late summer or late winter when temperature differences between SGD and the ocean waters are the largest ~3°C (Figs 7(a) and 8). During the spring and fall, SGD is about the same temperature as the ocean and would probably not be detected.

The success of a survey using thermal imagery can also be affected by the geology of the aquifer. When the aquifer is in direct hydraulic connection to the ocean, as in Case 1, a narrow zone of high discharge exists at the shoreline close to the surface. In this environment, the temperature difference of ~3ºC between the SGD and the ocean would probably be detected by an aerial survey using thermal imagery (Fig. 9). If there is a low conductivity layer of marine sediments producing a wide zone of discharge across the sea floor and a decreased amount of SGD, thermal imagery will likely not work. Even though the temperature difference is ~6ºC, the lack of concentrated discharge reaching the ocean surface would make SGD undetectable (Fig. 9). However, if there is a submarine spring in this environment, it would likely be identified by thermal imagery as long as the spring exists in shallow waters, there is an increased amount of SGD (i.e. at low tide), and the temperature difference is greater

than 0.08ºC (Fig. 9). If the submarine spring is too deep, thermal imagery will likely not detect the spring.

CONCLUSIONS

Numerical modelling can help enhance and guide SGD data collection efforts by providing estimates of expected salinity and temperature variations. Aerial surveys using EM resistivity are more appropriate for some coastal environments, whereas, thermal imagery is likely more successful in others. Results from this research indicate that modelling of a coastal environment prior to data collection can reveal the potential for success using either types of aerial surveys. This investigation also reveals that ignoring short-term temporal changes on the system, such as tides, could hinder modelling efforts to guide data collection. Although the results presented here appear to be representative for south Florida, the general conclusions may also be valid for other environments with similar hydrogeological and ocean characteristics.

REFERENCES

Bokuniewicz, H., Buddemeier, R., Maxwell, B. & Smith, C. (2003) The typological approach to submarine ground-water discharge (SGD). *Biogeochemistry* **66**, 145–158.

Dausman, A. & Langevin, C. D. (2005) Movement of the saltwater interface in the surficial aquifer system in response to hydrologic stresses and water-management practices, Broward County, Florida. *US Geol. Survey Scientific Investigations Report 2004-5256*.

Finkl, C. W. & Krupa, S. L. (2003) Environmental impacts of coastal-plain activities on sandy beach systems: hazards, perception and mitigation. *J. Coastal Res*. **35**, 132–150.

Langevin, C. D. (2003) Simulation of submarine ground water discharge to a marine estuary: Biscayne Bay, Florida. *Ground Water* **41**(6), 758–771.

Langevin, C. D., Shoemaker, W. B. & Guo, W. (2003) MODFLOW-2000: the US Geological Survey modular ground-water model. Documentation of the SEAWAT-2000 version with the variable-density flow process (VDF) and the integrated MT3DMS transport process (IMT). *US Geol. Survey Open-File Report 03-426*.

McDonald, M. G. & Harbaugh, A. W. (1988) A modular three-dimensional finite-difference ground-water flow model. *US Geol. Survey Techniques of Water Resources Investigations*, Book 6.

Michael, H. A., Mulligan, A. E. & Harvey, C. F. (2005) Seasonal oscillations in water exchange between aquifers and the coastal ocean. *Nature* **436**(6054), 1145-1148.

Smith, L. & Zawadski, W. (2003) A hydrologeologic model of submarine groundwater discharge: Florida intercomparison experiment. *Biogeochemistry* **66**, 95–110.

Taniguchi, M., Burnett, W. C., Cable, J. E. & Turner, J. V. (2002) Investigation of submarine groundwater discharge. *Hydrol. Processes* **16**, 2115–2129.

Thorne, D., Langevin, C. D. & Sukop, M. C. (2006) Addition of simultaneous heat and solute transport and variable fluid viscosity to SEAWAT. *Computers and Geosciences* **32**, 1758–1768.

Weiss, M., Kruse, S., Burnett, W. C., Chanton, J., Greenwood, W., Murray, M., Peterson, R. & Swarzenski, P. (2005) Evaluation of geophysical and thermal methods for detecting submarine groundwater discharge (SGD) in the Suwannee River Estuary. American Geophysical Union, Fall Meeting 2005, abstract #H43F-0554.

Wilson, A. M. (2005) Fresh and saline groundwater discharge to the ocean: a regional perspective. *Water Resour. Res.* **41**(2), 1–11.

Zheng, Chunmiao (1990) MT3D: A modular three-dimensional transport model for simulation of advection, dispersion and chemical reactions of contaminants in groundwater systems. Report to the US Environmental Protection Agency, Ada, Oklahoma, USA.